

# $X$ and $Z_{cs}$ in $B^+ \rightarrow J/\psi\phi K^+$ as $s$ -wave threshold cusps and alternative spin-parity assignments to $X(4274)$ and $X(4500)$

Xuan Luo<sup>1</sup> and Satoshi X. Nakamura<sup>2,3,\*</sup>

<sup>1</sup>*School of Physics and Optoelectronics Engineering,  
Anhui University, Hefei 230601, People's Republic of China*

<sup>2</sup>*University of Science and Technology of China, Hefei 230026, People's Republic of China*

<sup>3</sup>*State Key Laboratory of Particle Detection and Electronics (IHEP-USTC), Hefei 230036, People's Republic of China*

Recent LHCb's amplitude analysis on  $B^+ \rightarrow J/\psi\phi K^+$  suggests the existence of exotic  $X$  and  $Z_{cs}$  hadrons, based on an assumption that Breit-Wigner resonances describe all the peak structures. However, all the peaks and also dips in the spectra are located at relevant meson-meson thresholds where threshold kinematical cusps might cause such structures. This points to the importance of an independent amplitude analysis with due consideration of the kinematical effects, and this is what we do in this work. Our model fits well  $J/\psi\phi$ ,  $J/\psi K^+$ , and  $K^+\phi$  invariant mass distributions simultaneously, demonstrating that all the  $X$ ,  $Z_{cs}$ , and dip structures can be well described with the ordinary  $s$ -wave threshold cusps. Spin-parity of the  $X(4274)$  and  $X(4500)$  structures are respectively  $0^-$  and  $1^-$  from our model, as opposed to  $1^+$  and  $0^+$  from the LHCb's. With all relevant threshold cusps considered, the number of fitting parameters seems to be significantly reduced. The LHCb data requires  $D_s^{(*)}\bar{D}^*$  scattering lengths in our model to be consistent with zero, disfavoring  $D_s^{(*)}\bar{D}^*$  molecule interpretations of  $Z_{cs}(4000)$  and  $Z_{cs}(4220)$  and, via the SU(3) relation, being consistent with previous lattice QCD results.

*Introduction.*— Recent experimental developments resulted in many discoveries of new hadrons that are not categorized into the conventional  $qqq$  and  $q\bar{q}$  structures. Countless theoretical papers followed to understand the nature of such exotic hadrons often called  $XYZ$ , thereby deepening our knowledge of QCD in the nonperturbative regime; see reviews [1–3]. Hadron properties such as mass, width, and spin-parity ( $J^P$ ) are crucial information to address the hadrons' nature and structures, and amplitude analysis is the method to extract those information from data. However, amplitude analysis results are often neither unique nor model-independent for assumptions and simplifications that go into the analyses. It is therefore important to bring different and independent analysis results together to establish the hadron properties through critical reviews and comparisons.

The  $B^+ \rightarrow J/\psi\phi K^+$  decay<sup>1</sup> is an interesting case. Earlier analyses [5–12] fitted structures in the  $J/\psi\phi$  invariant mass ( $M_{J/\psi\phi}$ ) distribution with Breit-Wigner amplitudes, and claimed exotic  $X(4140)$  and  $X(4274)$  without  $J^P$  determinations. A first six-dimensional amplitude analysis was done by the LHCb Collaboration [13, 14], and four  $X$  states with  $J^P$  were reported:  $X(4140)$  and  $X(4274)$  with  $J^P = 1^+$ ;  $X(4500)$  and  $X(4700)$  with  $J^P = 0^+$ . These  $X$  states were confirmed with higher statistics data recently, and  $1^+X(4685)$ ,  $2^-X(4150)$ , and  $1^-X(4630)$  were also added [15]. Furthermore, the LHCb

claimed  $1^+cu\bar{c}\bar{s}$  tetraquarks  $Z_{cs}(4000)^+$  and  $Z_{cs}(4220)^+$  appearing as bumps in the  $M_{J/\psi K^+}$  distribution.

The LHCb's analysis assumes that all bumps in the  $M_{J/\psi\phi}$  and  $M_{J/\psi K^+}$  distributions are caused by  $X$  and  $Z_{cs}$  resonances that can be simulated by Breit-Wigner amplitudes. However, these  $X$  [ $Z_{cs}$ ] bumps and also dips are located at  $D_s^*\bar{D}_s^{(*)}$ ,  $D_{sJ}^{(*)}\bar{D}_s^{(*)}$ , and  $\psi'\phi$  [ $D_s^{(*)}\bar{D}^*$ ] thresholds where kinematical effects such as threshold cusps and/or triangle singularities may cause resonancelike and dip structures [16]. Indeed, it has been shown that  $X(4140)$  and  $X(4700)$  can be described with  $D_s^*\bar{D}_s$  and  $\psi'\phi$  threshold cusps, respectively [14, 17–21]. While  $1^+X(4274)$  [ $0^+X(4500)$ ] at the  $D_{s0}^*(2317)\bar{D}_s$  [ $D_{s1}(2536)\bar{D}_s$ ] threshold cannot be an ordinary  $s$ -wave cusp for having different  $J^P$ , they might still be described with  $p$ -wave cusps enhanced by quasi double-triangle singularities [21]. It is however noted that the LHCb's  $J^P$  assignments are not model-independent but influenced by their assumptions. Once possible threshold cusps not only at the peaks but also at the dips are considered in the fit, it is unclear whether the LHCb's  $J^P$  assignments remain unchanged. We address this issue.

Another issue concerns the nature of the  $Z_{cs}(4000)$  and  $Z_{cs}(4220)$ . A similar structure, called  $Z_{cs}(3985)$ , was also discovered by the BESIII collaboration in  $e^+e^- \rightarrow K^+(D_s^-D^{*0} + D_s^{*-}D^0)$  [22]. While  $Z_{cs}(4000)$  and  $Z_{cs}(3985)$  have similar masses ( $4003 \pm 6_{-14}^{+4}$  MeV and  $3982.5_{-2.6}^{+1.8} \pm 2.1$  MeV), their widths are rather different ( $131 \pm 15 \pm 26$  MeV and  $12.8_{-4.4}^{+5.3} \pm 3.0$  MeV); the first (second) errors are statistical (systematic).  $Z_{cs}(3985)$  and  $Z_{cs}(4000)$  are argued to be the same  $cu\bar{c}\bar{s}$  tetraquark state in Refs. [23, 24]. However, other works considered them to be different tetraquark states [25–28], or different  $D_s^{(*)}\bar{D}^{(*)}$  molecules [25, 29, 30], or one of them is a

<sup>1</sup> We follow the hadron naming scheme in Ref. [4]. We often denote  $J/\psi$  and  $\psi(2S)$  by  $\psi$  and  $\psi'$ , respectively, for simplicity.  $D_{s0}^*(2317)$  and  $D_{s1}(2536)$  are generically denoted by  $D_{sJ}^{(*)}$ . The charge conjugate decays are implied throughout, and charge indices are often suppressed.

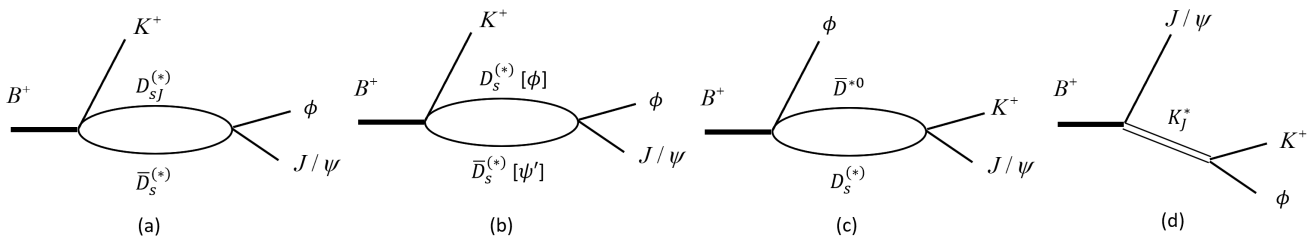


FIG. 1.  $B^+ \rightarrow J/\psi\phi K^+$  mechanisms: (a)  $D_{sJ}^{(*)+} D_s^{(*)-}$  ( $0^-, 1^-$ ) one-loop; (b)  $D_s^{*+} D_s^{*-}$  and  $\psi'\phi$  ( $0^+, 1^+$ ) one-loop; (c)  $D_s^{*+} \bar{D}^{*0}$  ( $1^+$ ) one-loop; (d)  $K_J^*$  ( $K, K^*, K_1, K_2$ ) excitations.

tetraquark and the other is a molecule [31].  $Z_{cs}(3985)$  and  $Z_{cs}(4000)$  may also be from a common virtual pole that enhances the  $D_s \bar{D}^*$  threshold cusp [32, 33], as demonstrated by fitting both the LHCb's  $M_{J/\psi K^+}$  distribution and BESIII data [32]. Also,  $J/\psi K^{*+}$  and  $\psi' K^+$  threshold cusps could cause the  $Z_{cs}(4000)$  and  $Z_{cs}(4220)$  structures, respectively [34].

$Z_{cs}(3985/4000)$  may be regarded as a SU(3) partner of  $Z_c(3900)$  [23, 26, 30, 32, 35, 36]. Lattice QCD (LQCD) results disfavor the existence of a narrow  $Z_c(3900)$  pole, suggesting  $Z_c(3900)$  to be a kinematical effect [37–41]. This implies, via the SU(3) relation, no pole for  $Z_{cs}(3985)$  and/or  $Z_{cs}(4000)$ . However, consistency with the LQCD results was not considered in most previous models<sup>2</sup>.

In this work, we develop a model that simultaneously describes the  $J/\psi\phi$ ,  $J/\psi K^+$ , and  $K^+\phi$  invariant mass distributions for  $B^+ \rightarrow J/\psi\phi K^+$  from the LHCb. We demonstrate that all the peaks ( $X, Z_{cs}$ ) and dips in the  $M_{J/\psi\phi}$  and  $M_{J/\psi K^+}$  distributions are well described with ordinary  $s$ -wave threshold cusps from one-loop diagrams in Fig. 1; virtual poles near the thresholds are not necessary for a good fit. Our model,  $J^P$  of the cusps as well, should be well-constrained by simultaneously fitting the three invariant mass distributions. Thus, we claim  $J^P = 0^-$  and  $1^-$  for the  $X(4274)$  and  $X(4500)$  cusps, respectively, alternative to  $J^P = 1^+$  and  $0^+$  from the LHCb analysis; the different  $J^P$  assignments would be from considering different mechanisms. We will argue possible advantages of our model over the LHCb's model. We also examine to what extent the  $D_s^{(*)} \bar{D}^*$  molecule interpretation of  $Z_{cs}(4000)$  and  $Z_{cs}(4220)$  is allowed by the LHCb data. The  $D_s^{(*)} \bar{D}^*$  scattering lengths in our model is required to be consistent with zero, disfavoring the molecule interpretation, and being consistent with the above-mentioned LQCD results.

*The model.*— We consider one-loop mechanisms of Fig. 1(a,b) [Fig. 1(c)] and their  $s$ -wave threshold cusps that generate structures in the  $M_{J/\psi\phi}$  [ $M_{J/\psi K^+}$ ] distribution of  $B^+ \rightarrow J/\psi\phi K^+$ . We also consider  $K_J^*$  excita-

tion mechanisms of Fig. 1(d) that would shape the  $M_{K^+\phi}$  distribution. We assume that other possible mechanisms play a minor role, and their effects can be effectively absorbed by the considered mechanisms. We derive the corresponding amplitudes by writing down effective Lagrangians of relevant hadrons and their matrix elements, and combining them following the time-ordered perturbation theory.

The one-loop mechanisms of Fig. 1(a) include  $s$ -wave pairs of

$$\begin{aligned} D_{s0}^*(2317)^+ D_s^-(0^-), \quad D_{s0}^*(2317)^+ D_s^{*-}(1^-), \\ D_{s1}(2536)^+ D_s^-(1^-), \quad D_{s1}(2536)^+ D_s^{*-}(0^-), \end{aligned} \quad (1)$$

where  $J^P$  of a pair is indicated in the parenthesis; a  $J^P = 0^-$  ( $1^-$ ) pair is from a parity-violating (conserving) weak decay. These mechanisms include short-range (e.g., quark-exchange)  $D_{sJ}^{(*)} \bar{D}_s^{(*)} \rightarrow J/\psi\phi$  interactions that would require a  $c\bar{s}$  component in  $D_{sJ}^{(*)}$ .  $D_{s1}(2536)$  is considered to be a  $p$ -wave  $c\bar{s}$  [44]. While  $D_{s0}^*(2317)$  may have a dominant  $DK$ -molecule component as found by analyzing LQCD energy spectrum [44–47], a bare  $c\bar{s}$  component can still be an important constituent [44]. The diagrams of Fig. 1(b) include  $s$ -wave pairs of

$$D_s^{*+} D_s^-(1^+), \quad D_s^{*+} D_s^{*-}(0^+), \quad \psi'\phi(0^+), \quad \psi'\phi(1^+), \quad (2)$$

where a  $J^P = 1^+$  ( $0^+$ ) pair is for a parity-violating (conserving) process. Since  $D_s^* \bar{D}_s^*(1^+)$  and  $J/\psi\phi(1^+)$  have different  $C$ -parity,  $D_s^* \bar{D}_s^*(1^+)$  does not contribute here. The diagrams of Fig. 1(c) include  $s$ -wave pairs of

$$D_s^+ \bar{D}^{*0}(1^+), \quad D_s^{*+} \bar{D}^{*0}(1^+), \quad (3)$$

that can contribute to both parity-conserving and violating processes. While a  $D_s^{*+} \bar{D}^0(1^+)$  one-loop mechanism is also possible, its singular behavior is similar to that of  $D_s^+ \bar{D}^{*0}(1^+)$  due to almost degenerate thresholds ( $\sim 1.8$  MeV difference). We thus assume that the  $D_s^+ \bar{D}^{*0}(1^+)$  one-loop amplitude implicitly absorbs the  $D_s^{*+} \bar{D}^0(1^+)$  contribution.

In Eqs. (1)-(3), we did not exhaust all possible  $J^P$  such as  $D_{s1}(2536)^+ D_s^{*-}(1^-, 2^-)$  and  $D_s^{*+} D_s^{*-}(2^+)$ . While they can in principle contribute to the process, we found them unnecessary to reasonably fit the three invariant

<sup>2</sup> An exception is Refs. [42, 43].

TABLE I.  $K_J^*$  in Fig. 1(d). The first row indicates  $J^P$  of  $K_J^*$ . In the default model, parity-conserving (pc) and/or -violating (pv) amplitudes or neither (-) are considered, as indicated in the square brackets.

$0^-$	$1^-$	$1^+$	$2^-$
$K(1460)[-]$	$K^*(1410)[pc]$ $K^*(1680)[pc]$	$K_1(1400)[-]$ $K_1(1650)[pc, pv]$	$K_2(1770)[pc]$ $K_2(1820)[pc]$

mass distributions. We thus do not consider them and keep the number of fitting parameters smaller. Also, we do not explicitly consider charge analogous amplitudes that include, for example,  $D_s^+ D_{s_0}^*(2317)^-$  rather than  $D_{s_0}^*(2317)^+ D_s^-$  in Fig. 1(a). While the charge analogous amplitudes generally have independent strengths, their singular behaviors are the same as the original ones. It is understood that their effects and projections onto positive  $C$ -parity are taken into account in coupling strengths of the considered processes.

We consider the  $K_J^*$ -excitation mechanisms of Fig. 1(d) in Breit-Wigner forms. With the LHCb's amplitude analysis result as reference, we consider  $K_J^*$  as listed in Table I. Each  $K_J^*$  may have parity-conserving and/or -violating  $B^+ \rightarrow K_J^* J/\psi$  couplings, depending on  $J^P$  of  $K_J^*$ .

We present an amplitude formula for Fig. 1(c) with a  $D_s^+ \bar{D}^{*0}(1^+)$  pair that generates a  $Z_{cs}(4000)$ -like cusp; see the Supplemental Material for amplitude formulas for other mechanisms. We denote the energy, width, three-momentum and polarization vector of a particle  $x$  by  $E_x$ ,  $\Gamma_x$ ,  $\vec{p}_x$  and  $\vec{\epsilon}_x$ , respectively. The particle masses and widths are taken from Ref. [4] unless otherwise stated. A parity-conserving (pc)  $B^+ \rightarrow D_s^+ \bar{D}^{*0} \phi$  vertex and the subsequent  $D_s^+ \bar{D}^{*0} \rightarrow J/\psi K^+$  interaction that enter the amplitude are

$$c_{D_s^+ \bar{D}^{*0}(1^+)}^{\text{pc}} \vec{\epsilon}_{\bar{D}^{*0}} \cdot \vec{\epsilon}_\phi F_{D_s^+ \bar{D}^{*0} \phi, B}^{00}, \quad (4)$$

$$c_{\psi K, D_s^+ \bar{D}^{*0}}^{1^+} \vec{\epsilon}_{\bar{D}^{*0}} \cdot \vec{\epsilon}_\psi f_{\psi K}^0 f_{D_s^+ \bar{D}^{*0}}^0, \quad (5)$$

respectively, where we introduced dipole form factors  $F_{ijk,l}^{LL'}$  and  $f_{ij}^L$ ; we use a common cutoff of  $\Lambda = 1$  GeV in all form factors;  $c_{D_s^+ \bar{D}^{*0}(1^+)}^{\text{pc}}$  and  $c_{\psi K, D_s^+ \bar{D}^{*0}}^{1^+}$  are coupling constants. With the above ingredients, the one-loop amplitude is given by

$$A_{\bar{D}^{*0} D_s(1^+)}^{1\text{L,pc}} = c_{\psi K, D_s^+ \bar{D}^{*0}}^{1^+} c_{D_s^+ \bar{D}^{*0}(1^+)}^{\text{pc}} \vec{\epsilon}_\psi \cdot \vec{\epsilon}_\phi \times \int d^3 p_{D_s} \frac{f_{\psi K}^0 f_{D_s^+ \bar{D}^{*0}}^0 F_{D_s^+ \bar{D}^{*0} \phi, B}^{00}}{M_{\psi K} - E_{D_s} - E_{\bar{D}^{*0}} + i\varepsilon}, \quad (6)$$

where  $\Gamma_{\bar{D}^{*0}}$  has been neglected for being estimated to be small ( $\Gamma_{\bar{D}^{*0}} \sim 55$  keV [48]).

The  $D_s^{(*)+} \bar{D}^{*0}$  threshold cusps from Eq. (6) could be enhanced by virtual or bound states near the thresholds [49]. To implement this effect, we describe

the  $D_s^{(*)+} \bar{D}^{*0} \rightarrow J/\psi K^+$  transition with a single-channel  $D_s^{(*)+} \bar{D}^{*0}$  scattering followed by a perturbative  $D_s^{(*)+} \bar{D}^{*0} \rightarrow J/\psi K^+$  transition. We use a  $D_s^{(*)+} \bar{D}^{*0}$  interaction potential of

$$v_\alpha(p', p) = f_\alpha^0(p') h_\alpha f_\alpha^0(p), \quad (7)$$

where  $\alpha$  labels an interaction channel;  $h_\alpha$  is a coupling constant and  $f_\alpha^L$  is a dipole form factor. We can implement the rescattering effect in Eq. (6) by multiplying  $[1 - h_\alpha \sigma_\alpha(M_{J/\psi K^+})]^{-1}$  with

$$\sigma_\alpha(E) = \int dq q^2 \frac{[f_\alpha^0(q)]^2}{E - E_{D_s}(q) - E_{\bar{D}^{*0}}(q) + i\varepsilon}. \quad (8)$$

The default model does not include the rescattering effects ( $h_\alpha = 0$ ) for Fig. 1(a,c). We will examine the rescattering effect on the  $Z_{cs}$  structures separately.

Meanwhile, our default model includes similar rescattering effects in the  $D_s^* \bar{D}_s^{(*)}$   $\rightarrow J/\psi \phi$  transitions of Fig. 1(b). The  $D_s^* \bar{D}_s^{(*)}$  interaction strengths are chosen to be moderately attractive ( $h_\alpha = -2$ ). The scattering length is  $a \sim 0.55$  fm<sup>3</sup>, and a virtual pole is located at  $\sim 20$  MeV below the  $D_s^* \bar{D}_s^{(*)}$  threshold. In Ref. [19], the authors used a contact  $D_s^* \bar{D}_s^{(*)}$  interaction saturated by a  $\phi$ -exchange mechanism, and found similar virtual poles.

*Results and discussions.*— We simultaneously fit the  $M_{J/\psi \phi}$ ,  $M_{J/\psi K^+}$ , and  $M_{K^+ \phi}$  distributions of  $B^+ \rightarrow J/\psi \phi K^+$  from the LHCb using the model described above. As seen in Eq. (6), each amplitude has a complex overall factor from the product of coupling constants. We determine the complex factors by fitting the data since other experimental inputs are lacking. During the fit, we remove relatively unimportant mechanisms to reduce the fitting parameters and retain essential mechanisms. For

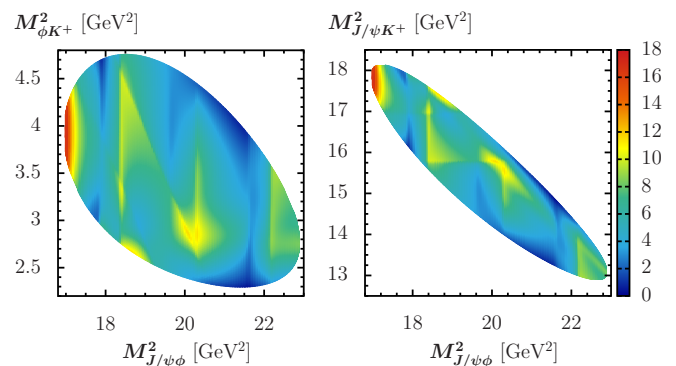


FIG. 2.  $B^+ \rightarrow J/\psi \phi K^+$  Dalitz plot distributions from the default model. No smearing is applied.

<sup>3</sup> The scattering length ( $a$ ) is related to the phase shift ( $\delta$ ) by  $p \cot \delta = 1/a + \mathcal{O}(p^2)$ .

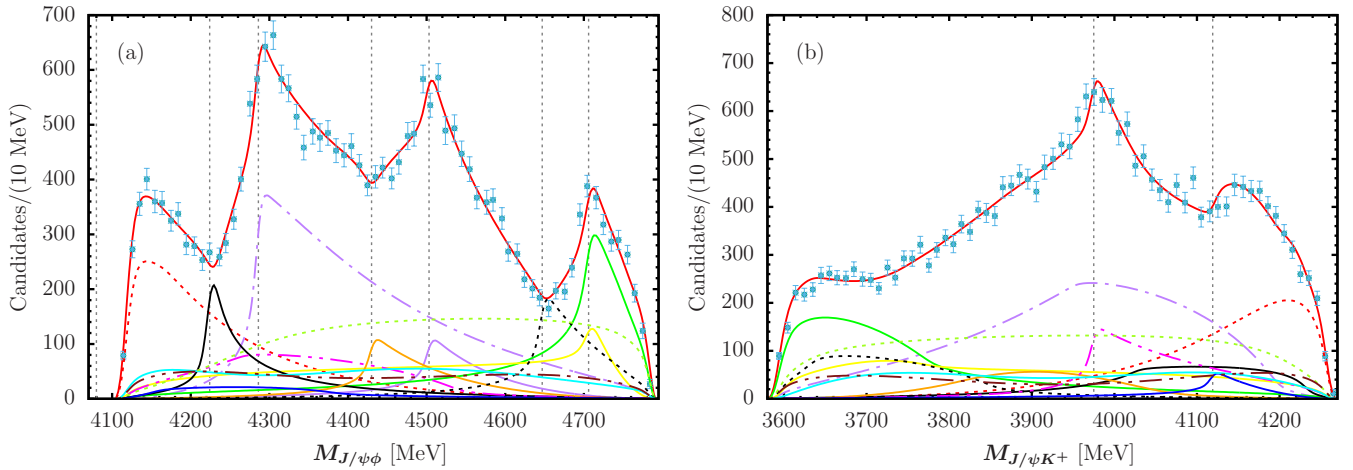


FIG. 3. Combined fit to (a)  $J/\psi\phi$ , (b)  $J/\psi K^+$ , and (c)  $\phi K^+$  invariant mass distributions for  $B^+ \rightarrow J/\psi\phi K^+$ . The red solid curves are from the default model. Contributions are from Fig. 1(a-c) that include  $D_s^{*+}D_s^-(1^+)$  [red dashed],  $D_s^{*+}D_s^{*-}(0^+)$  [black solid],  $D_{s0}^*(2317)^+D_s^-(0^-)$  [purple dash-dotted],  $D_{s0}^*(2317)^+D_s^{*-}(1^-)$  [orange solid],  $D_{s1}(2536)^+D_s^-(1^-)$  [purple solid],  $D_{s1}(2536)^+D_s^{*-}(0^-)$  [black dashed],  $\psi'\phi(0^+)$  [green solid],  $\psi'\phi(1^+)$  [yellow solid],  $D_s^+\bar{D}^{*0}(1^+)$  [magenta dash-two-dotted], and  $D_s^{*+}\bar{D}^{*0}(1^+)$  [blue solid]. Contributions from Fig. 1(d) are  $K^*$  [cyan solid],  $K_1$  [green dashed], and  $K_2$  [brown dash-two-dotted]. The dotted vertical lines in (a) [(b)] indicate thresholds for, from left to right,  $D_s^+\bar{D}_s$ ,  $D_s^+\bar{D}_s^*$ ,  $D_{s0}^*(2317)\bar{D}_s$ ,  $D_{s0}^*(2317)\bar{D}_s^*$ ,  $D_{s1}(2536)\bar{D}_s$ ,  $D_{s1}(2536)\bar{D}_s^*$ , and  $\psi'\phi$  [ $D_s^+\bar{D}^{*0}$  and  $D_s^{*+}\bar{D}^{*0}$ ], respectively. The data are from Ref. [15].

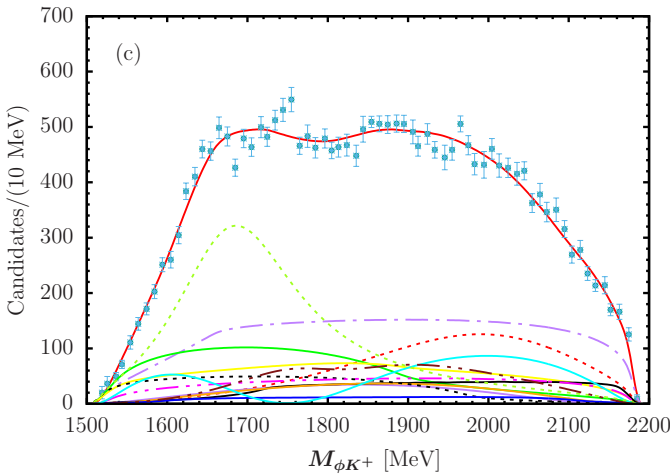


FIG. 4. Continued from Fig. 3.

Fig. 1(c) with Eq. (3), we remove a parity-violating [conserving] one with  $D_s^+\bar{D}^{*0}(1^+)$  [ $D_s^{*+}\bar{D}^{*0}(1^+)$ ]. Among the  $K_J^*$ -excitation mechanisms, we retain only those indicated by 'pc' and/or 'pv' in Table I. Our default model totally has 16 mechanisms, and  $2 \times 16 - 3 = 29$  fitting parameters where  $-3$  is from the arbitrariness of the absolute normalization of the full amplitude, and that of overall phases of the parity-conserving and -violating full amplitudes. The parameter values and fit fractions for the default model are provided in the Supplemental Material.

We first present Dalitz plot distributions from the de-

fault model in Fig. 2. Comparing with the LHCb's Dalitz plots [15], the overall patterns are similar. Since our plots are not smeared with the experimental resolution, the peak structures seem sharper than the data.

In Figs. 3 and 4, our default model (red solid curves) is shown to agree well with the LHCb data for the  $M_{J/\psi\phi}$ ,  $M_{J/\psi K^+}$ , and  $M_{K^+\phi}$  distributions;  $\chi^2/\text{ndf} = (102.3 + 94.2 + 113.7)/(3 \times 68 - 29) = 1.77$  where three  $\chi^2$  values are from the  $M_{J/\psi\phi}$ ,  $M_{J/\psi K^+}$ , and  $M_{K^+\phi}$  distributions, respectively, and ndf is the number of the bins subtracted by the number of fitting parameters. All theoretical curves are smeared with the experimental bin width. The  $X(4140)$ ,  $X(4274)$ ,  $X(4500)$ ,  $X(4700/4685)$  peaks in the  $M_{J/\psi\phi}$  distribution are well described by the  $D_s^{*+}D_s^-(1^+)$  [red dashed curve],  $D_{s0}^*(2317)^+D_s^-(0^-)$  [purple dash-dotted],  $D_{s1}(2536)^+D_s^-(1^-)$  [purple solid], and  $\psi'\phi(0^+/1^+)$  [green solid/yellow solid] threshold cusps, respectively. Also, the three dips are well fitted with the  $D_s^{*+}D_s^{*-}(0^+)$  [black solid],  $D_{s0}^*(2317)^+D_s^{*-}(1^-)$  [orange solid], and  $D_{s1}(2536)^+D_s^{*-}(0^-)$  [black dashed] threshold cusps. The cusp peak positions are slightly above the thresholds due to smearing the asymmetric cusp shapes.

In the  $M_{J/\psi K^+}$  distribution, the  $D_s^+\bar{D}^{*0}(1^+)$  threshold cusp [magenta dash-two-dotted] fits well the  $Z_{cs}(4000)$ -like peak. The  $D_s^{*+}\bar{D}^{*0}(1^+)$  threshold cusp [blue solid] creates a dip at  $M_{J/\psi K^+} \sim 4120$  MeV and, combined with the shrinking phase-space near the kinematical endpoint, the  $Z_{cs}(4220)$ -like structure is formed. While the  $K_J^*$ -excitation mechanisms do not create noticeable structures in the  $M_{K^+\phi}$  distribution, their contributions and

interferences are important for a reasonable fit.

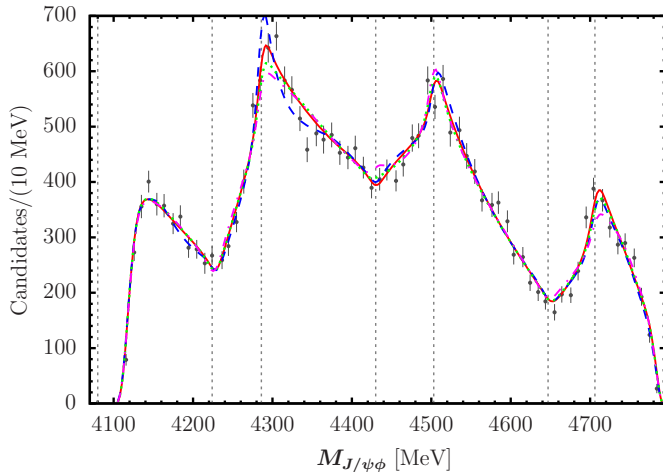


FIG. 5. The  $J/\psi\phi$  invariant mass distributions from the fits with different cutoff ( $\Lambda$ ) values in the dipole form factors. The blue dashed, red solid, green dotted, and magenta dash-dotted curves are obtained with  $\Lambda = 750, 1000, 1250,$  and  $1500$  MeV, respectively. Other features are the same as those in Fig. 3(a).

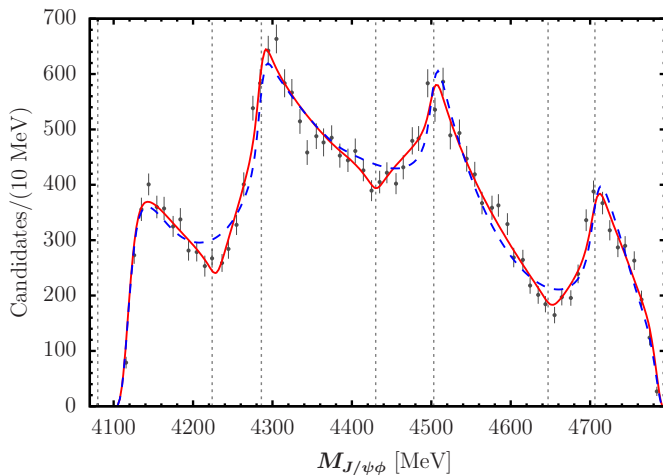


FIG. 6. The  $J/\psi\phi$  invariant mass distributions from the fits with different mechanisms. The red solid curve is from the default model. The blue dashed curve is from a model where the  $D_s^{*+}D_s^{*-}(0^+)$ ,  $D_{s0}^*(2317)^+D_s^{*-}(1^-)$ , and  $D_{s1}(2536)^+D_s^{*-}(0^-)$  loop mechanisms [Fig. 1(a,b)] are removed from the default mechanisms. Other features are the same as those in Fig. 3(a).

We examine if the fit is stable against changing the form factor. Instead of  $\Lambda = 1000$  MeV (cutoff) in all the dipole form factors of the default model, we fit the data with  $\Lambda = 750, 1250,$  and  $1500$  MeV. As seen in Fig. 5 for the  $M_{J/\psi\phi}$  distribution, while the sharpness of the  $X(4274)$  peak is somewhat sensitive to the cutoff value, the fit is reasonably stable overall. Similarly, stable fits

are also obtained for the  $M_{J/\psi K^+}$  and  $M_{K^+\phi}$  distributions. This stability is expected since the threshold cusps are caused by low-momentum components in the loop integrals, and are insensitive to how high-momentum components are cut off. We also used monopole and Gaussian form factors with  $\Lambda = 1$  GeV, and confirmed that the result is very similar to the case of  $\Lambda = 1250$  MeV in Fig. 5.

Our results are different from the LHCb's in many points. First, all  $X$  and  $Z_{cs}$  structures are from the threshold cusps in our model, while they are from resonances of the Breit-Wigner forms in the LHCb's. Second,  $J^P$  of the  $X(4274)$  and  $X(4500)$  peaks are respectively  $0^-$  and  $1^-$  cusps in our model while  $1^+$  and  $0^+$  resonances in the LHCb's. This difference in  $J^P$  might be from the fact that our model creates the sharp three dips in the  $M_{J/\psi\phi}$  distribution with the threshold cusps. In Fig. 6, we see that the dip regions are not well fitted with a model in which the threshold cusps at the dips are removed from the default setting [blue dashed]; adding more  $K_J^*$  in Table I does not help. On the other hand, the LHCb did not introduce resonances but use complicated interferences to fit the dip regions. Possibly due to this fitting choice, the LHCb amplitude model actually needs significantly more mechanisms and fitting parameters than our model does, as will be discussed shortly.

Another noteworthy point is that the LHCb's model includes a contact  $B^+ \rightarrow J/\psi\phi(1^+)K^+$  mechanism with a large ( $\sim 28\%$ ) fit fraction while our model does not. Since sequential two-body decay chains usually dominate, this large fit fraction could hint relevant missing mechanisms. Although our model also includes contact mechanisms such as  $B^+ \rightarrow D_{sJ}^{(*)}\bar{D}_s^{(*)}K^+, D_s^{(*)}\bar{D}^*\phi$  in Fig. 1(a-c), they can be understood as color-favored sequential two-body decay chains such as  $B^+ \rightarrow D_{s(J)}^{(*)}\bar{D}'$  followed by  $\bar{D}' \rightarrow \bar{D}_s^{(*)}K^+, \bar{D}^*\phi$ , and the off-shell excited charmed mesons ( $\bar{D}'$ ) in the loops can be shrunk to the contact mechanisms.

We also point out the difference in the number of fitting parameters ( $N_p$ ) and its implication. Our default model is fitted to the  $M_{J/\psi\phi}, M_{J/\psi K^+},$  and  $M_{K^+\phi}$  distributions with  $N_p = 29$ . The LHCb's amplitude model is fitted to the six-dimensional distribution with  $N_p = 144$  and, in comparison with the  $M_{J/\psi\phi}, M_{J/\psi K^+},$  and  $M_{K^+\phi}$  distributions,  $\chi^2 = 82.5, 79.4, 60.7,$  respectively. This large difference in  $N_p$  should be partly from the fact that the six-dimensional distribution include more information, and that the LHCb's fit quality is somewhat better. However, this might not fully explain the difference in  $N_p$ . Possibly, the LHCb's model misses relevant mechanisms and needs many others to mimic the missing ones through complicated interferences, resulting in the large  $N_p$ . At present, we cannot discuss which of the LHCb's model or ours is statistically more significant, since they were fitted to the different datasets.

Since the LHCb claimed  $X(4630)(1^-)$  and  $X(4150)(2^-)$ , we added them to our default model to see their relevance. Although the fit quality is slightly improved ( $\chi^2/\text{ndf} = 1.74$ ) a similar improvement can also be made by  $K_J^*$ -excitation mechanisms not included in the default model. We thus conclude that  $X(4630)(1^-)$  and  $X(4150)(2^-)$  are not relevant in our model and their importance seems model-dependent, as far as we fit the three invariant mass distributions.

Our default model fits well the  $Z_{cs}$ -like structures in the  $M_{J/\psi K^+}$  distribution with the threshold cusps without any poles nearby. We examine to what extent a molecule (pole) scenario for the  $Z_{cs}$  structures is allowed by the LHCb data. We vary the fitting parameters for Fig. 1(c) and also two independent  $D_s^+ \bar{D}^{*0}$  and  $D_s^{*+} \bar{D}^{*0}$  interaction strengths  $h_\alpha$  in Eq. (7), and find their allowed ranges. For the  $D_s^+ \bar{D}^{*0}$  scattering, we find  $-0.33 < h_\alpha < 0.93$  that corresponds to the scattering length of  $-0.12 < a(\text{fm}) < 0.06$ , and a virtual pole at 93 MeV below the threshold or deeper. Regarding the  $D_s^{*+} \bar{D}^{*0}$  scattering,  $-0.17 < h_\alpha < 2.02$ ,  $-0.21 < a(\text{fm}) < 0.03$ , and a virtual pole at 103 MeV below the threshold or deeper.

The result would disfavor the  $D_s^{(*)+} \bar{D}^{*0}$  molecules as an explanation for the  $Z_{cs}$  structures. Meanwhile, Ortega et al. [32] fitted well the  $M_{J/\psi K^+}$  distribution with  $D_s^{(*)+} \bar{D}^{*0}$  threshold cusps enhanced by virtual poles at 5–14 MeV below the thresholds. The difference from our result is partly from the fact that they used momentum-independent  $D_s^{(*)+} \bar{D}^{*0}$  production vertices while we used form factors. If we also use momentum-independent production vertices, we obtain, for the  $D_s^+ \bar{D}^{*0}$  scattering,  $-1.09 < h_\alpha < -0.25$ ,  $0.04 < a(\text{fm}) < 0.22$ , and a virtual pole at 48–99 MeV below the threshold. The molecule picture is still not clearly seen. To further examine the molecule scenario, Ref. [50] stressed the importance of considering also the elastic final state [e.g., the BESIII  $e^+e^- \rightarrow K^+(D_s^- D^{*0} + D_s^{*-} D^0)$  data [22] in the present context].

The LQCD results [37–41] suggested weak hadron-hadron interactions and neither bound nor narrow resonances in the channel for  $Z_c(3900)$  ( $J^{PC} = 1^{+-}$ ) and its  $1^{++}$  partner. Our results above, including the default model, are consistent with the LQCD results via the SU(3) relation; most of the previous  $Z_{cs}$  models did not take the consistency into account. Yet, a non-pole scenario has not well explained the experimentally observed peak structures [22, 51] that are commonly interpreted with the  $Z_c(3900)$  and  $Z_{cs}(3985)$  states. More works from experimental, phenomenological, and LQCD approaches are necessary to reach a consistent picture of  $Z_{c(s)}$ .

We thank F.-K. Guo for stimulating discussions and useful comments on the manuscript. We also acknowledge L. Zhang for useful information on the LHCb amplitude analysis. XL is supported by the National Natural Science Foundation of China under Grants No. 12205002, and SXN is supported by National Natural Science Foundation of China (NSFC) under contracts U2032103 and 11625523, and also by National Key Research and Development Program of China under Contracts 2020YFA0406400.

## Supplemental Material

### 1. Formulas for amplitudes in the default model

We present one-loop amplitudes of Fig. 1(a) that include  $s$ -wave  $D_{s0}^* \bar{D}_s(0^-)$ ,  $D_{s1} \bar{D}_s^*(0^-)$ ,  $D_{s0}^* \bar{D}_s^*(1^-)$  and  $D_{s1} \bar{D}_s(1^-)$ . The initial weak vertices  $B^+ \rightarrow D_{sJ}^{(*)} \bar{D}_s^{(*)} K^+$  are

$$c_{D_{s0}^* \bar{D}_s(0^-)} F_{D_{s0}^* \bar{D}_s K^+, B^+}^{00}, \quad (9)$$

$$c_{D_{s1} \bar{D}_s^*(0^-)} \vec{\epsilon}_{D_{s1}} \cdot \vec{\epsilon}_{\bar{D}_s^*} F_{D_{s1} \bar{D}_s^* K^+, B^+}^{00}, \quad (10)$$

$$c_{D_{s0}^* \bar{D}_s^*(1^-)} \vec{p}_{K^+} \cdot \vec{\epsilon}_{\bar{D}_s^*} F_{D_{s0}^* \bar{D}_s^* K^+, B^+}^{01}, \quad (11)$$

$$c_{D_{s1} \bar{D}_s(1^-)} \vec{p}_{K^+} \cdot \vec{\epsilon}_{\bar{D}_s} F_{D_{s1} \bar{D}_s K^+, B^+}^{01}, \quad (12)$$

and the subsequent  $D_{sJ}^{(*)} \bar{D}_s^{(*)} \rightarrow J/\psi \phi$  interactions are

$$c_{D_{s0}^* \bar{D}_s, \psi \phi}^{0-} i \vec{p}_\phi \cdot (\vec{\epsilon}_\psi \times \vec{\epsilon}_\phi) f_{\psi \phi}^1 f_{D_{s0}^* \bar{D}_s}^0, \quad (13)$$

$$c_{D_{s1} \bar{D}_s^*, \psi \phi}^{0-} \vec{\epsilon}_{D_{s1}} \cdot \vec{\epsilon}_{\bar{D}_s^*} i \vec{p}_\phi \cdot (\vec{\epsilon}_\psi \times \vec{\epsilon}_\phi) f_{\psi \phi}^1 f_{D_{s1} \bar{D}_s^*}^0, \quad (14)$$

$$c_{D_{s0}^* \bar{D}_s^*, \psi \phi}^{1-} (\vec{p}_\phi \times \vec{\epsilon}_{\bar{D}_s^*}) \cdot (\vec{\epsilon}_\psi \times \vec{\epsilon}_\phi) f_{\psi \phi}^1 f_{D_{s0}^* \bar{D}_s^*}^0, \quad (15)$$

$$c_{D_{s1} \bar{D}_s, \psi \phi}^{1-} (\vec{p}_\phi \times \vec{\epsilon}_{D_{s1}}) \cdot (\vec{\epsilon}_\psi \times \vec{\epsilon}_\phi) f_{\psi \phi}^1 f_{D_{s1} \bar{D}_s}^0, \quad (16)$$

respectively. We have introduced dipole form factors  $f_{ij}^L$ ,  $f_{ij,k}^L$ , and  $F_{ijk,l}^{LL'}$  given by

$$f_{ij}^L = \frac{1}{\sqrt{E_i E_j}} \left( \frac{\Lambda^2}{\Lambda^2 + q_{ij}^2} \right)^{2+(L/2)}, \quad (17)$$

$$f_{ij,k}^L = \frac{f_{ij}^L}{\sqrt{E_k}}, \quad (18)$$

$$F_{ijk,l}^{LL'} = \frac{f_{ij}^L f_{kl}^{L'}}{\sqrt{E_k E_l}} \left( \frac{\Lambda'^2}{\Lambda'^2 + \tilde{p}_k^2} \right)^{2+\frac{L'}{2}}, \quad (19)$$

where  $q_{ij}$  ( $\tilde{p}_k$ ) is the momentum of  $i$  ( $k$ ) in the  $ij$  (total) center-of-mass frame;  $\Lambda^{(l)}$  is a cutoff for which we use a common value of 1 GeV in all form factors. With the above ingredients, the one-loop amplitudes are given by

$$A_{D_{s0}^* \bar{D}_s(0^-)}^{1L} = c_{D_{s0}^* \bar{D}_s, \psi \phi}^{0-} c_{D_{s0}^* \bar{D}_s(0^-)} c_{D_{s0}^* \bar{D}_s} i \vec{p}_\phi \cdot (\vec{\varepsilon}_\psi \times \vec{\varepsilon}_\phi) \int d^3 p_{\bar{D}_s} \frac{f_{\psi \phi}^1 f_{D_{s0}^* \bar{D}_s}^0 F_{D_{s0}^* \bar{D}_s K^+, B^+}^{00}}{M_{\psi \phi} - E_{D_{s0}^*} - E_{\bar{D}_s} + i\varepsilon}, \quad (20)$$

$$A_{D_{s1} \bar{D}_s^*(0^-)}^{1L} = 3c_{D_{s1} \bar{D}_s^*, \psi \phi}^{0-} c_{D_{s1} \bar{D}_s^*(0^-)} i \vec{p}_\phi \cdot (\vec{\varepsilon}_\psi \times \vec{\varepsilon}_\phi) \int d^3 p_{\bar{D}_s^*} \frac{f_{\psi \phi}^1 f_{D_{s1} \bar{D}_s^*}^0 F_{D_{s1} \bar{D}_s^* K^+, B^+}^{00}}{M_{\psi \phi} - E_{D_{s1}} - E_{\bar{D}_s^*} + i\varepsilon}, \quad (21)$$

$$A_{D_{s0}^* \bar{D}_s^*(1^-)}^{1L} = c_{D_{s0}^* \bar{D}_s^*, \psi \phi}^{1-} c_{D_{s0}^* \bar{D}_s^*(1^-)} (\vec{p}_\phi \times \vec{p}_{K^+}) \cdot (\vec{\varepsilon}_\psi \times \vec{\varepsilon}_\phi) \int d^3 p_{\bar{D}_s^*} \frac{f_{\psi \phi}^1 f_{D_{s0}^* \bar{D}_s^*}^0 F_{D_{s0}^* \bar{D}_s^* K^+, B^+}^{01}}{M_{\psi \phi} - E_{D_{s0}^*} - E_{\bar{D}_s^*} + i\varepsilon}, \quad (22)$$

$$A_{D_{s1} \bar{D}_s^*(1^-)}^{1L} = c_{D_{s1} \bar{D}_s^*, \psi \phi}^{1-} c_{D_{s1} \bar{D}_s^*(1^-)} (\vec{p}_\phi \times \vec{p}_{K^+}) \cdot (\vec{\varepsilon}_\psi \times \vec{\varepsilon}_\phi) \int d^3 p_{\bar{D}_s^*} \frac{f_{\psi \phi}^1 f_{D_{s1} \bar{D}_s^*}^0 F_{D_{s1} \bar{D}_s^* K^+, B^+}^{01}}{M_{\psi \phi} - E_{D_{s1}} - E_{\bar{D}_s^*} + i\varepsilon}. \quad (23)$$

Similarly, one-loop amplitudes of Fig. 1(b) that include

$s$ -wave  $D_s^* \bar{D}_s(1^+)$ ,  $D_s^* \bar{D}_s^*(0^+)$ , and  $\psi' \phi(0^+, 1^+)$  are given by

$$A_{D_s^* \bar{D}_s(1^+)}^{1L} = c_{\psi \phi, D_s^* \bar{D}_s}^{1+} c_{D_s^* \bar{D}_s(1^+)} i (\vec{\varepsilon}_\psi \times \vec{\varepsilon}_\phi) \cdot \vec{p}_{K^+} \int d^3 p_{\bar{D}_s} \frac{f_{\psi \phi}^0 f_{D_s^* \bar{D}_s}^0 F_{D_s^* \bar{D}_s K^+, B}^{01}}{M_{\psi \phi} - E_{D_s^*} - E_{\bar{D}_s} + i\varepsilon}, \quad (24)$$

$$A_{D_s^* \bar{D}_s^*(0^+)}^{1L} = 3c_{\psi \phi, D_s^* \bar{D}_s^*}^{0+} c_{D_s^* \bar{D}_s^*(0^+)} \vec{\varepsilon}_\psi \cdot \vec{\varepsilon}_\phi \int d^3 p_{\bar{D}_s^*} \frac{f_{\psi \phi}^0 f_{D_s^* \bar{D}_s^*}^0 F_{D_s^* \bar{D}_s^* K^+, B}^{00}}{M_{\psi \phi} - E_{D_s^*} - E_{\bar{D}_s^*} + i\varepsilon}, \quad (25)$$

$$A_{\psi' \phi(0^+)}^{1L} = 3c_{\psi \phi, \psi' \phi}^{0+} c_{\psi' \phi(0^+)} \vec{\varepsilon}_\psi \cdot \vec{\varepsilon}_\phi \int d^3 p_{\psi'} \frac{f_{\psi \phi}^0 f_{\psi' \phi}^0 F_{\psi' \phi K^+, B}^{00}}{M_{\psi \phi} - E_{\psi'} - E_\phi + \frac{i}{2} \Gamma_\phi}, \quad (26)$$

$$A_{\psi' \phi(1^+)}^{1L} = 2c_{\psi \phi, \psi' \phi}^{1+} c_{\psi' \phi(1^+)} i (\vec{\varepsilon}_\psi \times \vec{\varepsilon}_\phi) \cdot \vec{p}_{K^+} \int d^3 p_{\psi'} \frac{f_{\psi \phi}^0 f_{\psi' \phi}^0 F_{\psi' \phi K^+, B}^{01}}{M_{\psi \phi} - E_{\psi'} - E_\phi + \frac{i}{2} \Gamma_\phi}, \quad (27)$$

respectively;  $\Gamma_{\psi'}$  has been neglected since  $\Gamma_{\psi'} \ll \Gamma_\phi$ .

Next we present one-loop amplitudes of Fig. 1(c) that include  $s$ -wave  $D_s \bar{D}^{*0}(1^+)$  and  $D_s^* \bar{D}^{*0}(1^+)$ . While parity-conserving and -violating weak decays can initiate the processes, our default model includes parity-conserving  $D_s \bar{D}^{*0}(1^+)$  and parity-violating  $D_s^* \bar{D}^{*0}(1^+)$  one-loop amplitudes. The weak  $B^+ \rightarrow D_s^{(*)} \bar{D}^{*0} \phi$  vertices included in these amplitudes are

$$c_{D_s \bar{D}^{*0}(1^+)}^{\text{pc}} \vec{\varepsilon}_{\bar{D}^{*0}} \cdot \vec{\varepsilon}_\phi F_{D_s \bar{D}^{*0} \phi, B}^{00}, \quad (28)$$

$$c_{D_s^* \bar{D}^{*0}(1^+)}^{\text{pv}} (\vec{\varepsilon}_{\bar{D}^{*0}} \times \vec{\varepsilon}_{D_s^*}) \cdot (\vec{p}_\phi \times \vec{\varepsilon}_\phi) F_{D_s^* \bar{D}^{*0} \phi, B}^{01}, \quad (29)$$

where superscripts pc and pv indicate parity-conserving and parity-violating, respectively. The subsequent  $D_s^{(*)} \bar{D}^{*0} \rightarrow J/\psi K^+$  interactions are given by

$$c_{K^+ \psi, D_s \bar{D}^{*0}}^{1+} \vec{\varepsilon}_{\bar{D}^{*0}} \cdot \vec{\varepsilon}_\psi f_{K^+ \psi}^0 f_{D_s \bar{D}^{*0}}^0, \quad (30)$$

$$c_{K^+ \psi, D_s^* \bar{D}^{*0}}^{1+} i (\vec{\varepsilon}_{\bar{D}^{*0}} \times \vec{\varepsilon}_{D_s^*}) \cdot \vec{\varepsilon}_\psi f_{K^+ \psi}^0 f_{D_s^* \bar{D}^{*0}}^0. \quad (31)$$

With the above ingredients, the one-loop amplitudes are

$$A_{D_s \bar{D}^{*0}(1^+)}^{1L, \text{pc}} = c_{K^+ \psi, D_s \bar{D}^{*0}}^{1+} c_{D_s \bar{D}^{*0}(1^+)}^{\text{pc}} \vec{\varepsilon}_\psi \cdot \vec{\varepsilon}_\phi \int d^3 p_{D_s} \frac{f_{K^+ \psi}^0 f_{D_s \bar{D}^{*0}}^0 F_{D_s \bar{D}^{*0} \phi, B}^{00}}{M_{\psi K^+} - E_{\bar{D}^{*0}} - E_{D_s} + i\varepsilon}, \quad (32)$$

$$A_{D_s^* \bar{D}^{*0}(1^+)}^{1L, \text{pv}} = -2c_{K^+ \psi, D_s^* \bar{D}^{*0}}^{1+} c_{D_s^* \bar{D}^{*0}(1^+)}^{\text{pv}} i (\vec{\varepsilon}_\psi \times \vec{\varepsilon}_\phi) \cdot \vec{p}_\phi \int d^3 p_{D_s^*} \frac{f_{K^+ \psi}^0 f_{D_s^* \bar{D}^{*0}}^0 F_{D_s^* \bar{D}^{*0} \phi, B}^{01}}{M_{\psi K^+} - E_{\bar{D}^{*0}} - E_{D_s^*} + i\varepsilon}. \quad (33)$$

Now we present formulas for  $K_J^*$ -excitation mecha-

nisms of Fig. 1(d); see Table 1 for  $K_J^*$  considered in our



default model. For  $1^-K^*$ , our default model includes a parity-conserving amplitude given by

$$A_{K^*}^{\text{pc}} = c_{K^*}^{\text{pc}} \frac{(\vec{p}_\psi \times \vec{\varepsilon}_\psi) \cdot (\vec{p}_\phi \times \vec{\varepsilon}_\phi) f_{\phi K^+, K^*}^1 f_{K^* \psi, B}^1}{E - E_\psi - E_{K^*} + \frac{i}{2} \Gamma_{K^*}}, \quad (34)$$

where  $K^*$  is either  $K^*(1410)$  or  $K^*(1680)$ .

As for  $1^+K_1$ , we consider both parity-conserving and -violating amplitudes given as

$$A_{K_1}^{\text{pc}} = c_{K_1}^{\text{pc}} \frac{\vec{\varepsilon}_\psi \cdot \vec{\varepsilon}_\phi f_{\phi K^+, K_1}^0 f_{K_1 \psi, B}^0}{E - E_\psi - E_{K_1} + \frac{i}{2} \Gamma_{K_1}}, \quad (35)$$

$$A_{K_1}^{\text{pv}} = c_{K_1}^{\text{pv}} \frac{i(\vec{\varepsilon}_\psi \times \vec{\varepsilon}_\phi) \cdot \vec{p}_\psi f_{\phi K^+, K_1}^0 f_{K_1 \psi, B}^1}{E - E_\psi - E_{K_1} + \frac{i}{2} \Gamma_{K_1}}, \quad (36)$$

respectively, with  $K_1 = K_1(1650)$ .

Regarding  $2^-K_2$ , our default model includes a parity-conserving amplitude given by

$$A_{K_2}^{\text{pc}} = c_{K_2}^{\text{pc}} \frac{f_{\phi K^+, K_2}^1 f_{\psi K_2, B^+}^1}{E - E_\psi - E_{K_2} + \frac{i}{2} \Gamma_{K_2}} \left( \frac{1}{2} \vec{\varepsilon}_\phi \cdot \vec{p}_\psi \vec{\varepsilon}_\psi \cdot \vec{p}_\phi + \frac{1}{2} \vec{\varepsilon}_\phi \cdot \vec{\varepsilon}_\psi \vec{p}_\phi \cdot \vec{p}_\psi - \frac{1}{3} \vec{\varepsilon}_\phi \cdot \vec{p}_\phi \vec{\varepsilon}_\psi \cdot \vec{p}_\psi \right), \quad (37)$$

where  $K_2$  is either  $K_2(1770)$  or  $K_2(1820)$ .

In practice, we calculate amplitudes of Eqs. (20)-(27) [Eqs. (32) and (33)] in the  $J/\psi\phi$  [ $J/\psi K^+$ ] center-of-mass frame. The  $K_J^*$ -excitation amplitudes of Eqs. (34)-(37) are calculated in the total center-of-mass frame, but the second  $K_J^{*+} \rightarrow K^+\phi$  vertices are calculated in the  $K^+\phi$  center-of-mass frame, as in the helicity formalism employed by the LHCb analysis. The invariant amplitudes are obtained from the above-presented amplitudes by multiplying relevant kinematical factors, and are plugged into the Dalitz plot distribution formula; see Appendix B of Ref. [52] for details.

Parameter values obtained from the fit are listed in Table II. The masses and widths appearing in the above formulas are taken from Ref. [4]. In Table II, we also list each mechanism's fit fraction defined by

$$\text{FF} = \frac{\Gamma_{A_x}}{\Gamma_{\text{full}}} \times 100(\%), \quad (38)$$

where  $\Gamma_{\text{full}}$  and  $\Gamma_{A_x}$  are  $B^+ \rightarrow J/\psi\phi K^+$  decay rates calculated with the default model and with an amplitude  $A_x$  only, respectively.

---

\* satoshi@ustc.edu.cn

- [1] H.-X. Chen, W. Chen, X. Liu, and S.-L. Zhu, The hidden-charm pentaquark and tetraquark states, *Phys. Rep.* **639**, 1 (2016).  
 [2] S.L. Olsen, T. Skwarnicki, and D. Zieminska, Nonstandard heavy mesons and baryons: Experimental evidence, *Rev. Mod. Phys.* **90**, 015003 (2018).

- [3] N. Brambilla, S. Eidelman, C. Hanhart, A. Nefediev, C.-P. Shen, C.E. Thomas, A. Vairo, and C.-Z. Yuan, The  $XYZ$  states: Experimental and theoretical status and perspectives, *Phys. Rept.* **873**, 1 (2020).  
 [4] P.A. Zyla et al. (Particle Data Group), The Review of Particle Physics, *Prog. Theor. Exp. Phys.* **2020**, 083C01 (2020).  
 [5] T. Aaltonen et al. (CDF Collaboration), Evidence for a Narrow Near-Threshold Structure in the  $J/\psi\phi$  Mass Spectrum in  $B^+ \rightarrow J/\psi\phi K^+$  Decays, *Phys. Rev. Lett.* **102**, 242002 (2009).  
 [6] J. Brodzicka, Heavy flavour spectroscopy, *Conference Proceedings C0908171*, 299 (2009).  
 [7] T. Aaltonen et al. (CDF Collaboration), Observation of the  $Y(4140)$  structure in the  $J/\psi\phi$  mass spectrum in  $B^\pm \rightarrow J/\psi\phi K$  decays, *Mod. Phys. Lett. A* **32**, 1750139 (2017).  
 [8] R. Aaij et al. (LHCb Collaboration), Search for the  $X(4140)$  state in  $B^+ \rightarrow J/\psi\phi K^+$  decays, *Phys. Rev. D* **85**, 091103(R) (2012).  
 [9] S. Chatrchyan et al. (CMS Collaboration), Observation of a peaking structure in the  $J/\psi\phi$  mass spectrum from  $B^\pm \rightarrow J/\psi\phi K^\pm$  decays, *Phys. Lett. B* **734**, 261 (2014).  
 [10] V.M. Abazov et al. (D0 Collaboration), Search for the  $X(4140)$  state in  $B^+ \rightarrow J/\psi\phi K^+$  decays with the D0 detector, *Phys. Rev. D* **89**, 012004 (2014).  
 [11] J.P. Lees et al. (BABAR Collaboration), Study of  $B^{\pm,0} \rightarrow J/\psi K^+ K^- K^{\pm,0}$  and search for  $B^0 \rightarrow J/\psi\phi$  at BABAR, *Phys. Rev. D* **91**, 012003 (2015).  
 [12] V.M. Abazov et al. (D0 Collaboration), Inclusive Production of the  $X(4140)$  State in  $p\bar{p}$  Collisions at D0, *Phys. Rev. Lett.* **115**, 232001 (2015).  
 [13] R. Aaij et al. (LHCb Collaboration), Observation of  $J/\psi\phi$  Structures Consistent with Exotic States from Amplitude Analysis of  $B^+ \rightarrow J/\psi\phi K^+$  Decays, *Phys. Rev. Lett.* **118**, 022003 (2017).  
 [14] R. Aaij et al. (LHCb Collaboration), Amplitude analysis of  $B^+ \rightarrow J/\psi\phi K^+$  decays, *Phys. Rev. D* **95**, 012002 (2017).  
 [15] R. Aaij et al. (LHCb Collaboration), Observation of new resonances decaying to  $J/\psi K^+$  and  $J/\psi\phi$ , *Phys. Rev. Lett.* **127**, 082001 (2021).  
 [16] F.-K. Guo, X.-H. Liu, and S. Sakai, Threshold cusps and triangle singularities in hadronic reactions, *Prog. Part. Nucl. Phys.* **112**, 103757 (2020).  
 [17] P.G. Ortega, J. Segovia, D.R. Entem, and F. Fernández, Canonical description of the new LHCb resonances, *Phys. Rev. D* **94**, 114018 (2016).  
 [18] X.-H. Liu, How to understand the underlying structures of  $X(4140)$ ,  $X(4274)$ ,  $X(4500)$  and  $X(4700)$ , *Phys. Lett. B* **766**, 117 (2017).  
 [19] X.-K. Dong, F.-K. Guo, and B.-S. Zou, A survey of heavy-antiheavy hadronic molecules, *Progr. Phys.* **41**, 65 (2021).  
 [20] E.S. Swanson, Cusps and Exotic Charmonia, *Int. J. Mod. Phys. E* **25**, 1642010 (2016).  
 [21] S.X. Nakamura,  $X$  structures in  $B^+ \rightarrow J/\psi\phi K^+$  as one-loop and double-triangle threshold cusps, arXiv:2111.05115 [hep-ph].  
 [22] M. Ablikim et al. (BESIII Collaboration), Observation of a Near-Threshold Structure in the  $K^+$  Recoil-Mass Spectra in  $e^+e^- \rightarrow K^+(D_s^- D^{*0} + D_s^{*-} D^0)$ , *Phys. Rev. Lett.* **126**, 102001 (2021).  
 [23] P.-P. Shi, F. Huang, and W.-L. Wang, Hidden charm



TABLE II. Parameter values and fit fractions for the default model ( $\Lambda = 1$  GeV) obtained from fitting the LHCb data [15]. The first column lists each mechanism considered in our model, and the second column is its fit fraction (%) defined in Eq.(38). The third column lists the product of coupling constants to fit the data, and its value and unit are given in the fourth and fifth columns, respectively. Amplitude formulas are given in the equations in the last column.

$A_{D_{s0}^* \bar{D}_s(0^-)}^{1L}$	33.3	$c_{D_{s0}^* \bar{D}_s, \psi \phi}^{0-} c_{D_{s0}^* \bar{D}_s(0^-)}$	$-15.0 + 14.4 i$	GeV <sup>-1</sup>	Eq. (20)
$A_{D_{s1} \bar{D}_s^*(0^-)}^{1L}$	8.0	$c_{D_{s1} \bar{D}_s^*, \psi \phi}^{0-} c_{D_{s1} \bar{D}_s^*(0^-)}$	$0.06 + 4.32 i$	GeV <sup>-1</sup>	Eq. (21)
$A_{D_{s0}^* \bar{D}_s^*(1^-)}^{1L}$	5.6	$c_{D_{s0}^* \bar{D}_s^*, \psi \phi}^{1-} c_{D_{s0}^* \bar{D}_s^*(1^-)}$	$-14.0 - 21.4 i$	GeV <sup>-2</sup>	Eq. (22)
$A_{D_{s1} \bar{D}_s(1^-)}^{1L}$	5.2	$c_{D_{s1} \bar{D}_s, \psi \phi}^{1-} c_{D_{s1} \bar{D}_s(1^-)}$	$21.6 + 10.8 i$	GeV <sup>-2</sup>	Eq. (23)
$A_{D_s^* \bar{D}_s(1^+)}^{1L}$	16.5	$c_{\psi \phi, D_s^* \bar{D}_s}^{1+} c_{D_s^* \bar{D}_s(1^+)}$	$12.7 + 2.26 i$	GeV <sup>-1</sup>	Eq. (24)
$A_{D_s^* \bar{D}_s^*(0^+)}^{1L}$	7.4	$c_{\psi \phi, D_s^* \bar{D}_s^*}^{0+} c_{D_s^* \bar{D}_s^*(0^+)}$	$0.08 + 1.24 i$	—	Eq. (25)
$A_{\psi' \phi(0^+)}^{1L}$	15.1	$c_{\psi \phi, \psi' \phi}^{0+} c_{\psi' \phi(0^+)}$	4.04	—	Eq. (26)
$A_{\psi' \phi(1^+)}^{1L}$	14.4	$c_{\psi \phi, \psi' \phi}^{1+} c_{\psi' \phi(1^+)}$	$16.6 - 2.14 i$	GeV <sup>-1</sup>	Eq. (27)
$A_{D_s^* \bar{D}^{*0}(1^+)}^{1L,pc}$	9.8	$c_{K^+ \psi, D_s^* \bar{D}^{*0}}^{1+} c_{D_s^* \bar{D}^{*0}(1^+)}^{pc}$	$-3.34 - 3.56 i$	—	Eq. (32)
$A_{D_s^* \bar{D}^{*0}(1^+)}^{1L,pv}$	2.4	$c_{K^+ \psi, D_s^* \bar{D}^{*0}}^{1+} c_{D_s^* \bar{D}^{*0}(1^+)}^{pv}$	$2.97 i$	GeV <sup>-1</sup>	Eq. (33)
$A_{K^*(1680)}^{pc}$	37.5	$c_{K^*(1680)}^{pc}$	$-28.4 + 38.0 i$	—	Eq. (34)
$A_{K^*(1410)}^{pc}$	49.1	$c_{K^*(1410)}^{pc}$	$-25.4 - 62.6 i$	—	Eq. (34)
$A_{K_1(1650)}^{pc}$	10.9	$c_{K_1(1650)}^{pc}$	$0.97 + 2.41 i$	GeV <sup>2</sup>	Eq. (35)
$A_{K_1(1650)}^{pv}$	18.8	$c_{K_1(1650)}^{pv}$	$5.93 + 1.06 i$	GeV <sup>1</sup>	Eq. (36)
$A_{K_2(1770)}^{pc}$	9.0	$c_{K_2(1770)}^{pc}$	$-24.3 + 6.03 i$	—	Eq. (37)
$A_{K_2(1820)}^{pc}$	20.0	$c_{K_2(1820)}^{pc}$	$31.9 + 23.4 i$	—	Eq. (37)

tetraquark states in a diquark model, Phys. Rev. D **103**, 094038 (2021).

- [24] J.F. Giron, R.F. Lebed, and S.R. Martinez, Spectrum of hidden-charm, open-strange exotics in the dynamical diquark model, Phys. Rev. D **104**, 054001 (2021).
- [25] Q.-N. Wang, W. Chen, and H.-X. Chen, Exotic molecular states and tetraquark states with  $J^P = 0^+, 1^+, 2^+$ , Chin. Phys. C **45**, 093102 (2021).
- [26] L. Maiani, A.D. Polosa, and V. Riquer, The new resonances  $Z_{cs}(3985)$  and  $Z_{cs}(4003)$  (almost) fill two tetraquark nonets of broken  $SU(3)_f$ , Sci. Bull. **66**, 1616 (2021).
- [27] J.-B. Wang, G. Li, C.-S. An, C.-R. Deng, and J.-J. Xie, The low-lying hidden- and double-charm tetraquark states in a constituent quark model with Instanton-induced Interaction, arXiv:2204.13320 [hep-ph].
- [28] M. Karliner and J.L. Rosner, Configuration mixing in strange tetraquarks  $Z_{cs}$ , Phys. Rev. D **104**, 034033 (2021).
- [29] S. Han and L.-Y. Xiao, Aspects of  $Z_{cs}(3985)$  and  $Z_{cs}(4000)$ , Phys. Rev. D **105**, 054008 (2022).
- [30] L. Meng, B. Wang, G.-J. Wang, and S.-L. Zhu, Implications of the  $Z_{cs}(3985)$  and  $Z_{cs}(4000)$  as two different states, Sci. Bull. **66**, 2065 (2021).
- [31] Z.-G. Wang, The decay widths of the  $Z_{cs}(3985/4000)$  based on rigorous quark-hadron duality, arXiv:2205.03203 [hep-ph].
- [32] P.G. Ortega, D.R. Entem, and F. Fernández, The strange partner of the  $Z_c$  structures in a coupled-channels model, Phys. Lett. B **818**, 136382 (2021).
- [33] Z. Yang, X. Cao, F.-K. Guo, J. Nieves, and M.P. Valderama, Strange molecular partners of the  $Z_c(3900)$  and  $Z_c(4020)$ , Phys. Rev. D **103**, 074029 (2021).
- [34] Y.-H. Ge, X.-H. Liu, and H.-W. Ke, Threshold effects as the origin of  $Z_{cs}(4000)$ ,  $Z_{cs}(4220)$  and  $X(4700)$  observed in  $B^+ \rightarrow J/\psi \phi K^+$ , Eur. Phys. J. C **81**, 854 (2021).
- [35] M.-L. Du, M. Albaladejo, F.-K. Guo, and J. Nieves, Combined analysis of the  $Z_c(3900)$  and the  $Z_{cs}(3985)$  exotic states, Phys. Rev. D **105**, 074018 (2022).
- [36] V. Baru, E. Epelbaum, A.A. Filin, C. Hanhart, and A.V. Nefediev, Is  $Z_{cs}(3982)$  a molecular partner of  $Z_c(3900)$  and  $Z_c(4020)$  states?, Phys. Rev. D **105**, 034014 (2022).
- [37] S. Prelovsek and L. Leskovec, Search for  $Z_c^+(3900)$  in the  $1^{+-}$  channel on the lattice, Phys. Lett. **B727**, 172 (2013).
- [38] Y. Chen, M. Gong, Y.-H. Lei, N. Li, J. Liang, C. Liu et al., Low-energy scattering of the  $(D\bar{D}^*)^\pm$  system and the resonance-like structure  $Z_c(3900)$ , Phys. Rev. D **89**, 094506 (2014).
- [39] S. Prelovsek, C.B. Lang, L. Leskovec, and D. Mohler, Study of the  $Z_c^+$  channel using lattice QCD, Phys. Rev. D **91**, 014504 (2015).
- [40] Y. Ikeda, S. Aoki, T. Doi, S. Gongyo, T. Hatsuda, T. Inoue, T. Iritani, N. Ishii, K. Murano, and K. Sasaki, Fate of the Tetraquark Candidate  $Z_c(3900)$  from Lattice QCD, Phys. Rev. Lett. **117**, 242001 (2016).
- [41] G.K.C. Cheung, C.E. Thomas, J.J. Dudek, and R.G. Ed-

- wards, Tetraquark operators in lattice QCD and exotic flavour states in the charm sector, *JHEP* **11**, 033 (2017).
- [42] M. Albaladejo, F.-K. Guo, C. Hidalgo-Duque, and J. Nieves,  $Z_c(3900)$ : What has been really seen?, *Phys. Lett.* **B755**, 337 (2016).
- [43] M. Albaladejo, P. Fernandez-Soler, and J. Nieves,  $Z_c(3900)$ : Confronting theory and lattice simulations, *Eur. Phys. J. C* **76**, 573 (2016).
- [44] Z. Yang, G.-J. Wang, J.-J. Wu, M. Oka, and S.-L. Zhu, Novel coupled channel framework connecting quark model and lattice QCD: an investigation on near-threshold  $D_s$  states, *Phys. Rev. Lett.* **128**, 112001 (2022).
- [45] L. Liu, K. Orginos, F.-K. Guo, C. Hanhart, and U.-G. Meißner, Interactions of charmed mesons with light pseudoscalar mesons from lattice QCD and implications on the nature of the  $D_{s0}^*(2317)$  *Phys. Rev. D* **87**, 014508 (2013).
- [46] A. Martínez Torres, E. Oset, S. Prelovsek, and A. Ramos, Reanalysis of lattice QCD spectra leading to the  $D_{s0}^*(2317)$  and  $D_{s1}^*(2460)$ , *JHEP* **05**, 153 (2015).
- [47] G.K.C. Cheung, C.E. Thomas, D.J. Wilson, G. Moir, M. Peardon, and S.M. Ryan (Hadron Spectrum Collaboration),  $DK$   $I = 0$ ,  $D\bar{K}$   $I = 0, 1$  scattering and the  $D_{s0}^*(2317)$  from lattice QCD, *JHEP* **02**, 100 (2021).
- [48] S.X. Nakamura, Triangle singularity appearing as an  $X(3872)$ -like peak in  $B \rightarrow (J/\psi\pi^+\pi^-)K\pi$ , *Phys. Rev. D* **102**, 074004 (2020).
- [49] X.-K. Dong, F.-K. Guo, and B.-S. Zou, Explaining the Many Threshold Structures in the Heavy-Quark Hadron Spectrum, *Phys. Rev. Lett.* **126**, 152001 (2021).
- [50] F.-K. Guo, C. Hanhart, Q. Wang, and Q. Zhao, Could the near-threshold  $XYZ$  states be simply kinematic effects?, *Phys. Rev. D* **91**, 051504(R) (2015).
- [51] M. Ablikim et al. (BESIII Collaboration), Determination of the Spin and Parity of the  $Z_c(3900)$ , *Phys. Rev. Lett.* **119**, 072001 (2017).
- [52] H. Kamano, S.X. Nakamura, T.S. Lee, and T. Sato, Unitary coupled-channels model for three-mesons decays of heavy mesons, *Phys. Rev. D* **84**, 114019 (2011).